Proceedings of the 45th IEEE Conference on Decision & Control
Manchester Grand Hyatt Hotel
San Diego, CA, USA, December 13-15, 2006

Transition control using an array of streamwise vortices

Rashad Moarref and Mihailo R. Jovanović

Abstract— **In this paper, we assess effectiveness of using an array of counter-rotating streamwise vortices for transition control in channel flows. We develop models that govern the dynamics of velocity perturbations in the presence of body force excitations and show how changes in control parameters affect perturbation kinetic energy. Effectively, we establish that high frequency streamwise vortices result in the largest energy amplification reduction. Our findings complement a numerical study of Schoppa & Hussain [1] and provide theoretical guidelines for a design of efficient turbulence suppression strategies.**

I. Introduction

Sensorless flow control is a promising technology for implementation, as it represents a much simpler alternative to feedback flow control with distributed wall-mounted arrays of sensors and actuators. In this paper, we study the energy of velocity perturbations in channel flows subject to an array of counter-rotating streamwise vortices. Our approach complements the numerical results of Schoppa & Hussain [1], and provides a system-theoretic framework for design of efficient sensorless transition control strategies. Since the transition (to turbulence) in channel flows is not appropriately captured by the eigenvalue analysis [2]–[9], we conduct an input-output analysis of stochastically excited linearized Navier-Stokes (NS) equations. Our analysis quantifies the effect of imposed streamwise vortices on velocity perturbations and furnishes systematic guidelines to optimal selection of control parameters for preventing transition.

Our subsequent development is organized as follows: in section II we determine a linearization of the NS equations around the plane channel flow subject to an additional array of counter-rotating streamwise vortices. An appropriate frequency representation of the streamwise constant three-dimensional linearized model is presented in § II-B. A brief overview of the notion of *frequency response* of linear spatially periodic systems is given in § II-C. A computationally efficient method for determination of the $\mathcal{H}_2$ norm in the presence of small amplitude oscillations is discussed in § III. This method was originally developed by Fardad & Bamieh [10], [11], and it is extended in this paper to account for the higher order corrections to the $\mathcal{H}_2$ norm. In § IV, we employ perturbation analysis to identify the oscillation frequencies that lead to the largest $\mathcal{H}_2$ norm reduction for streamwise constant perturbations. Effectively, we show that high frequency streamwise vortices result in the largest energy amplification reduction. We also derive an explicit dependence of the $\mathcal{H}_2$ norm with the Reynolds number R. We summarize our presentation in § V and provide a brief outlook for future research directions.

R. Moarref and M. R. Jovanović are with the Department of Electrical and Computer Engineering, University of Minnesota, Minneapolis, MN 55455, USA (e-mails: rashad@umn.edu, mihailo@umn.edu).

Supported in part by the Office of the Dean of the Graduate School of the University of Minnesota Grant-in-Aid of Research, Artistry and Scholarship Award 1546-522-5985.

II. Linearized Navier-Stokes equations

Consider a channel flow of an incompressible fluid with geometry illustrated in Fig. 1. The dynamics of velocity and pressure fluctuations $(\mathbf{v}, p)$ around some nominal flow condition $(\bar{\mathbf{u}}, \bar{P})$ are described by the linearized NS and continuity equations

$$\begin{aligned} \mathbf{v}_t &= -\boldsymbol{\nabla}_{\bar{\mathbf{u}}}\mathbf{v} - \boldsymbol{\nabla}_{\mathbf{v}}\bar{\mathbf{u}} - \boldsymbol{\nabla}p + \tfrac{1}{R}\Delta\mathbf{v} + \mathbf{d}, \\ 0 &= \boldsymbol{\nabla}\cdot\mathbf{v}. \end{aligned} \tag{1}$$

The spatial coordinates and velocities in (1) are normalized by channel half-width δ and largest nominal streamwise velocity U_m, respectively, and the Reynolds number R is given by $R := U_m\delta/\nu$, where ν denotes the kinematic viscosity. Operator $\boldsymbol{\nabla}$ represents the gradient, $\Delta := \boldsymbol{\nabla}\cdot\boldsymbol{\nabla}$ is the Laplacian, and $\boldsymbol{\nabla}_{\bar{\mathbf{u}}}$ is defined as $\boldsymbol{\nabla}_{\bar{\mathbf{u}}} := \bar{\mathbf{u}}\cdot\boldsymbol{\nabla}$. System (1) is driven by the body force fluctuation vector $\mathbf{d} := \begin{bmatrix} d_1 & d_2 & d_3 \end{bmatrix}^T$.

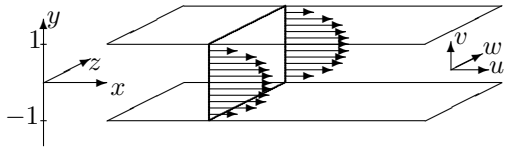

Fig. 1. Three dimensional plane channel flow.

We assume the nominal velocity of the form

$$\bar{\mathbf{u}} := \begin{bmatrix} U(y) & V(y,z) & W(y,z) \end{bmatrix}^T, \tag{2}$$

where $U(y)$ denotes the plane channel flow, i.e. $U(y) := 1 - y^2$, and

$$\begin{aligned} V(y,z) &:= 2\,\alpha\,\Omega\,\bar{V}(y)\cos(\Omega z), \\ W(y,z) &:= 2\,\alpha\,\bar{W}(y)\sin(\Omega z), \\ \bar{V}(y) &:= -(1+\cos(\pi y)), \\ \bar{W}(y) &:= -\bar{V}_y(y) = -\pi\sin(\pi y). \end{aligned} \tag{3}$$

Here, α and Ω are positive constants denoting the non-dimensional amplitude and the spanwise frequency of the applied flow, respectively. If W_m represents the largest nominal spanwise velocity then $\alpha = R_w/R$, where R_w is the Reynolds number defined in terms of W_m, $R_w := W_m\delta/\nu$. Note that $\bar{\mathbf{u}}$ satisfies the continuity equation. Since the nominal vorticity is determined by

$$\bar{\boldsymbol{\omega}} := \nabla\times\bar{\mathbf{u}} = \begin{bmatrix} W_y - V_z & 0 & -U_y \end{bmatrix}^T,$$

the flow given by (3) can be visualized as an array of counter-rotating two-dimensional streamwise vortices.

The wall-normal and spanwise components of $\bar{\mathbf{u}}$ given by (3) are introduced by Schoppa & Hussain [1]. The direct numerical simulations showed that a significant drag reduction can be obtained by super-imposing $V(y,z)$ and $W(y,z)$ to a fully developed turbulent channel flow [1]. In this paper, we study how (3) influences evolution of velocity fluctuations $\mathbf{v} := \left[\begin{array}{ccc} u & v & w \end{array}\right]^T$ in *transitional* channel flows. We develop a system theoretic framework for selection of amplitude and frequency of spanwise oscillations and show that the approach of Schoppa & Hussain can be also employed to control transition to turbulence.

A. Streamwise constant model

In this paper, we study the externally excited linearized NS equations in the presence of streamwise constant three-dimensional perturbations. This model is usually referred to as the 2D/3C model, and it is obtained by assuming the x-independence for all fields in (1), e.g. $\mathbf{d} = \mathbf{d}(y,z,t)$. In other words, all derivatives in (1) with respect to x are set to zero, i.e. $\partial_x(\cdot) \equiv 0$. Here, 2D stands for two-dimensional (in the (y,z)-plane), and 3C stands for three velocity perturbation components (u, v, w).

There are several reasons for a careful study of the 2D/3C model. An overwhelming body of theoretical and numerical evidence suggests that the streamwise constant perturbations create the largest contribution to the kinetic energy. Thus, any control strategy should be evaluated on the 2D/3C model to determine whether the energy amplification increases or decreases compared to the uncontrolled flow.

The state-space representation of the streamwise constant system (1) is obtained by applying a standard transformation to the wall-normal velocity (v)/vorticity (η) formulation

$$\begin{aligned} E\,\boldsymbol{\psi}_t(y,z,t) &= F\,\boldsymbol{\psi}(y,z,t) + G\,\mathbf{d}(y,z,t), \\ \mathbf{v}(y,z,t) &= C\,\boldsymbol{\psi}(y,z,t), \end{aligned} \tag{4}$$

where $\boldsymbol{\psi} := \left[\begin{array}{cc} v & \eta \end{array}\right]^T = \left[\begin{array}{cc} v & u_z \end{array}\right]^T$, and

$$v(\pm 1,z,t) = v_y(\pm 1,z,t) = \eta(\pm 1,z,t) = 0,\ z \in \mathbb{R},\ t \geq 0.$$

Operators E, G, and C do not depend on $\bar{\mathbf{u}}$ and their structure will be specified shortly. On the other hand, F is a 2×2 block-operator whose elements depend on the underlying nominal velocity. In particular, for $\bar{\mathbf{u}}$ given by (2) we have

$$\begin{aligned} F_{11} &= (1/R)\Delta^2 + (V_y - V\partial_y - W\partial_z)\Delta + \\ &\quad \big((\Delta V) - V_z\partial_z + (\Delta V_z)\partial_z^{-1}\big)\,\partial_y + \\ &\quad (\Delta W)\partial_z - (\Delta V_y) - V_z\partial_z^{-1}\partial_{yyy}, \\ F_{22} &= (1/R)\Delta - W_z - W\partial_z - (V + V_z\partial_z^{-1})\partial_y, \\ F_{21} &= -U_y\partial_z, \quad F_{12} = 0. \end{aligned}$$

Note that ∂_y and ∂_z represent differential operators in the wall-normal and spanwise directions, respectively, and ∂_z^{-1} is a symbol for the integral operator in z, i.e.

$$\partial_z^{-1} : f \mapsto g \quad \Leftrightarrow \quad f = \partial_z g =: g_z.$$

Furthermore, for $V(y,z)$ and $W(y,z)$ determined by (3), F can be represented as

$$F = F_0 + 2\alpha\left(\cos(\Omega z)F_c + \sin(\Omega z)F_s\right), \tag{5}$$

where F_0, F_c, and F_s denote operators that are spatially invariant in the spanwise direction. The Fourier symbols of these operators are given by

$$\begin{aligned} F_0(k_z) &:= \left[\begin{array}{cc} (1/R)\Delta^2 & 0 \\ -\mathrm{j}k_zU_y & (1/R)\Delta \end{array}\right], \\ F_r(k_z) &:= \left[\begin{array}{cc} F_{r11}(k_z) & 0 \\ 0 & F_{r22}(k_z) \end{array}\right], \\ F_{c11}(k_z) &:= \Omega(\bar{V}_y - \bar{V}\partial_y)\Delta + \Omega(\bar{V}_{yy} - \Omega^2\bar{V})\partial_y + \\ &\quad \Omega(\bar{W}_{yy} - \Omega^2\bar{W}), \\ F_{s11}(k_z) &:= \mathrm{j}k_z\big(\bar{W}_{yy} - \bar{W}(\Delta + \Omega^2 I)\big) + \\ &\quad \mathrm{j}(\Omega^2/k_z)\big(\bar{V}_{yy} - \bar{V}(\Delta + \Omega^2 I)\big)\partial_y, \\ F_{c22}(k_z) &:= \Omega(\bar{V}_y - \bar{V}\partial_y), \\ F_{s22}(k_z) &:= \mathrm{j}\big(k_z\bar{V}_y - (\Omega^2/k_z)\bar{V}\partial_y\big), \end{aligned}$$

where k_z is the spanwise wave-number, and $\mathrm{j} := \sqrt{-1}$. Operators E, G, and C are also spatially invariant in z, as evident from their Fourier symbols

$$E(k_z) := \left[\begin{array}{cc} \Delta & 0 \\ 0 & I \end{array}\right],\ C(k_z) := \left[\begin{array}{cc} 0 & -\mathrm{j}/k_z \\ I & 0 \\ (\mathrm{j}/k_z)\partial_y & 0 \end{array}\right],$$
$$G(k_z) := \left[\begin{array}{ccc} 0 & -k_z^2 & -\mathrm{j}k_z\partial_y \\ \mathrm{j}k_z & 0 & 0 \end{array}\right].$$

With a slight abuse of notation we use the same notation for Δ and Δ^2 in the physical and frequency domains. Note that in the frequency domain $\Delta := \partial_{yy} - k_z^2$, with homogenous Dirichlet boundary conditions, and $\Delta^2 := \partial_{yyyy} - 2k_z^2\partial_{yy} + k_z^4$, with homogenous Dirichlet *and* Neumann boundary conditions. A complete description of the underlying spaces and domains of these operator can be found in [5], [12].

B. Frequency representation of the 2D/3C model

The 2D/3C model represents a system of partial integro-differential equations in two spatial directions (y,z) and time, with the coefficients determined by $\bar{\mathbf{u}}$. In particular, for the nominal velocity (2,3), this set of equations has the periodic coefficients in z. Using a method for representation of spatially periodic operators in the frequency domain [13], we rewrite (4) in a form suitable for input-output analysis

$$\begin{aligned} \partial_t\boldsymbol{\psi}_\theta(y,t) &= \mathcal{A}_\theta\,\boldsymbol{\psi}_\theta(y,t) + \mathcal{B}_\theta\,\mathbf{d}_\theta(y,t), \\ \mathbf{v}_\theta(y,t) &= \mathcal{C}_\theta\,\boldsymbol{\psi}_\theta(y,t). \end{aligned} \tag{6}$$

System (4) is rendered into (6) using a unitary *lifting* transformation which preserves both stability properties and input-output system norms. Note that (6) represents a family of decoupled infinite dimensional systems parameterized by $\theta \in [0,\ \Omega)$.

For any triple (θ,y,t), $\{\boldsymbol{\psi}_\theta(y,t),\ \mathbf{d}_\theta(y,t),\ \mathbf{v}_\theta(y,t)\}$ denote bi-infinite vectors whose nth components are, respectively, obtained by evaluating $\{\boldsymbol{\psi}(y,k_z,t),\ \mathbf{d}(y,k_z,t),\ \mathbf{v}(y,k_z,t)\}$ at $k_z = \theta + n\Omega =: \theta_n$, $n \in \mathbb{Z}$. Here, $\boldsymbol{\psi}(y,k_z,t)$ represents a Fourier transform of $\boldsymbol{\psi}(y,z,t)$, i.e.

$$\boldsymbol{\psi}(y,k_z,t) := \int_{-\infty}^{\infty} \boldsymbol{\psi}(y,z,t)\,\mathrm{e}^{-\mathrm{j}zk_z}\,\mathrm{d}z,$$

and, thus

$$\boldsymbol{\psi}_\theta(y,t) := \mathrm{col}\,\{\boldsymbol{\psi}(y,\theta+n\Omega,t)\}_{n\,\in\,\mathbb{Z}}.$$

On the other hand, $\mathcal{A}_\theta$, $\mathcal{B}_\theta$, and $\mathcal{C}_\theta$ denote bi-infinite operator-valued matrices whose structure will be specified shortly. These matrices can be determined from the following two special cases [13]:

- A *spatially invariant* operator G with a Fourier symbol $G(k_z)$ has a block-diagonal matrix representation

  $$\mathcal{G}_\theta \;:=\; \mathrm{diag}\,\{G(\theta+n\Omega)\}_{n\in\mathbb{Z}} \;=:\; \mathrm{diag}\,\{G(\theta_n)\}_{n\in\mathbb{Z}}\,.$$

  For example, spatially invariant operators $\{E,\, F_0,\, F_r,\, F_c, G, C\}$ in (4,5) have block-diagonal representations.
- A *periodic pure multiplication* operator $T(z)$ with Fourier series coefficients $\{T_n\}_{n\in\mathbb{Z}}$ has a θ-independent block-Toeplitz matrix representation

  $$\mathcal{T}_\theta \;:=\; \mathrm{toep}\left\{\cdots, T_2, T_1, \boxed{T_0}, T_{-1}, T_{-2}, \cdots\right\},$$

  where the box denotes the element on the main diagonal of $\mathcal{T}_\theta$. For example, if $T(z) := \cos(\Omega z)$, then $\mathcal{T}_\theta = (1/2)\Gamma_c$, where Γ_c is a block-Toeplitz operator with $\{T_{\pm1} = I;\, T_n = 0,\, n \neq \pm1\}$; if $T(z) := \sin(\Omega z)$, then $\mathcal{T}_\theta = (\mathrm{j}/2)\Gamma_s$, where Γ_s is a block-Toeplitz operator with $\{T_1 = -I,\, T_{-1} = I;\, T_n = 0,\, n \neq \pm1\}$.

A matrix representation of the sums and cascades of spatially invariant and periodic pure multiplication operators is readily determined from these special cases. For example, for operator F in (5) we have

$$\mathcal{F}_\theta \;=\; \mathcal{F}_{0\theta} \,+\, \alpha\left(\Gamma_c\mathcal{F}_{c\theta} \,+\, \mathrm{j}\Gamma_s\mathcal{F}_{s\theta}\right),$$

where, for $r = \{0,c,s\}$, $\mathcal{F}_{r\theta}$ denote block-diagonal operators, $\mathcal{F}_{r\theta} := \mathrm{diag}\,\{F_r(\theta_n)\}_{n\in\mathbb{Z}}$. Thus, $\mathcal{A}_\theta$, $\mathcal{B}_\theta$, $\mathcal{C}_\theta$ in (6) are determined by

$$\begin{aligned}
\mathcal{A}_\theta \;&:=\; \mathcal{E}_\theta^{-1}\mathcal{F}_\theta \;=:\; \mathcal{A}_{0\theta} \,+\, \alpha\mathcal{A}_{1\theta},\\
\mathcal{A}_{0\theta} \;&:=\; \mathcal{E}_\theta^{-1}\mathcal{F}_{0\theta} \;=\; \mathrm{diag}\,\{E^{-1}(\theta_n)\,F_0(\theta_n)\}_{n\in\mathbb{Z}} \;=:\\
&\qquad \mathrm{diag}\,\{A_0(\theta_n)\}_{n\in\mathbb{Z}}\\
\mathcal{A}_{1\theta} \;&:=\; \mathcal{E}_\theta^{-1}\Gamma_c\mathcal{F}_{c\theta} \,+\, \mathrm{j}\mathcal{E}_\theta^{-1}\Gamma_s\mathcal{F}_{s\theta},\\
\mathcal{B}_\theta \;&:=\; \mathcal{E}_\theta^{-1}\mathcal{G}_\theta \;=\; \mathrm{diag}\,\{E^{-1}(\theta_n)\,G(\theta_n)\}_{n\in\mathbb{Z}} \;=:\\
&\qquad \mathrm{diag}\,\{B(\theta_n)\}_{n\in\mathbb{Z}},\quad \mathcal{C}_\theta \;:=\; \mathrm{diag}\,\{C(\theta_n)\}_{n\in\mathbb{Z}},
\end{aligned}$$

where we used the fact that $\mathcal{E}_\theta := \mathrm{diag}\,\{E(\theta_n)\}_{n\in\mathbb{Z}}$ is invertible. For a convenience of later algebraic manipulations we rewrite $\mathcal{A}_{1\theta}$ as

$$\mathcal{A}_{1\theta} \;=\; \mathcal{S}_1\,\mathrm{diag}\,\{A_{-1}(\theta_n)\}_{n\in\mathbb{Z}} \,+\, \mathrm{diag}\,\{A_1(\theta_n)\}_{n\in\mathbb{Z}}\,\mathcal{S}_1^*,$$

where $\mathcal{S}_1 := \mathrm{toep}\,\{\cdots, 0, 0, \boxed{0}, I, 0, \cdots\}$, and

$$\begin{aligned}
A_{-1}(\theta_n) \;&:=\; E^{-1}(\theta_{n-1})\left(F_c(\theta_n) \,+\, \mathrm{j}F_s(\theta_n)\right),\\
A_1(\theta_n) \;&:=\; E^{-1}(\theta_n)\left(F_c(\theta_{n-1}) \,-\, \mathrm{j}F_s(\theta_{n-1})\right).
\end{aligned}$$

C. Frequency response of the 2D/3C model

We next define the *frequency response* of the 2D/3C model, and introduce a notion of the $\mathcal{H}_2$ norm. An in-depth treatment of frequency responses and input-output system gains for spatially periodic systems is contained in [13].

The frequency response of the 2D/3C model is obtained by evaluating the transfer function of (6) on the jω-axis

$$\mathcal{H}_\theta(\omega) \;=\; \mathcal{C}_\theta(\mathrm{j}\omega\mathcal{I} \,-\, \mathcal{A}_\theta)^{-1}\mathcal{B}_\theta,$$

where $\omega \in \mathbb{R}$ denotes the temporal frequency, and $\mathcal{I}$ is the bi-infinite identity operator. For any value of (ω,θ), $\mathcal{H}_\theta(\omega)$ is an operator that relates the temporal Fourier transforms of bi-infinite input and output vectors $\mathbf{d}_\theta(y,t)$ and $\mathbf{v}_\theta(y,t)$

$$\mathbf{v}_\theta(y,\omega) \;=\; [\mathcal{H}_\theta(\omega)\,\mathbf{d}_\theta(\omega)](y).$$

Equivalently, the frequency response of a stable spatially periodic system can be interpreted in terms of *exponentially modulated periodic* (EMP) signals. The spatial EMP signals represent the appropriate test functions for spatially periodic systems; namely, the steady-state response of (4) to a spatial EMP signal

$$\mathbf{d}(y,z,t) \;=\; \mathrm{e}^{\mathrm{j}\theta z}\,\bar{\mathbf{d}}(y,z,t) \;=\; \sum_{n=-\infty}^{\infty} \bar{\mathbf{d}}_n(y,t)\,\mathrm{e}^{\mathrm{j}(\theta+n\Omega)z},$$

is also a spatial EMP signal

$$\mathbf{v}(y,z,t) \;=\; \mathrm{e}^{\mathrm{j}\theta z}\,\bar{\mathbf{v}}(y,z,t) \;=\; \sum_{n=-\infty}^{\infty} \bar{\mathbf{v}}_n(y,t)\,\mathrm{e}^{\mathrm{j}(\theta+n\Omega)z}.$$

Here, $\bar{\mathbf{d}}(y,z,t)$ and $\bar{\mathbf{v}}(y,z,t)$ denote the $2\pi/\Omega$ periodic functions in z, and $\{\bar{\mathbf{d}}_n(y,t),\, \bar{\mathbf{v}}_n(y,t)\}$ are the coefficients in the Fourier series expansions of $\{\bar{\mathbf{d}}(y,z,t),\, \bar{\mathbf{v}}(y,z,t)\}$. The frequency response of (4) is an operator that maps a bi-infinite vector $\mathrm{col}\,\{\bar{\mathbf{d}}_n(y,\omega)\}_{n\in\mathbb{Z}}$ to a bi-infinite vector $\mathrm{col}\,\{\bar{\mathbf{v}}_n(y,\omega)\}_{n\in\mathbb{Z}}$.

Note that, for each pair of (ω,θ), $\mathcal{H}_\theta(\omega)$ represents a bi-infinite matrix whose elements are one-dimensional operators in y. This infinite dimensional object contains a large amount of information about the behavior of the linearized NS system. The dynamical properties of (4) are often easier to visualize by introducing certain scalar quantities that compare the relative sizes of the inputs and the outputs. Amongst the various input-output amplification measures, the $\mathcal{H}_2$ norm is one of the most vastly used. For spatially periodic systems, the $\mathcal{H}_2$ norm is determined by [13]

$$\begin{aligned}
\|\mathcal{H}\|_2^2 \;&:=\; \frac{1}{2\pi}\int_0^\Omega \int_{-\infty}^{\infty} \mathrm{trace}\,\left(\mathcal{H}_\theta(\omega)\mathcal{H}_\theta^*(\omega)\right)\,\mathrm{d}\omega\,\mathrm{d}\theta\\
&=\; \frac{1}{2\pi}\int_0^\Omega \mathrm{trace}\,\left(\mathcal{P}_\theta\mathcal{C}_\theta^*\mathcal{C}_\theta\right)\,\mathrm{d}\theta,
\end{aligned}$$

where $\mathcal{P}_\theta$ represents the solution to the following operator Lyapunov equation

$$\mathcal{A}_\theta\mathcal{P}_\theta \,+\, \mathcal{P}_\theta\mathcal{A}_\theta^* \;=\; -\,\mathcal{B}_\theta\mathcal{B}_\theta^*. \tag{7}$$

For block-diagonal operators $\mathcal{C}_\theta$, the $\mathcal{H}_2$ norm can be expressed as

$$\begin{aligned}
\|\mathcal{H}\|_2^2 \;&=\; \frac{1}{2\pi}\sum_{n=-\infty}^{\infty}\int_0^\Omega \mathrm{trace}\,\left(P_d(\theta_n)C^*(\theta_n)C(\theta_n)\right)\,\mathrm{d}\theta\\
&=\; \frac{1}{2\pi}\int_{-\infty}^{\infty} \mathrm{trace}\,\left(P_d(k_z)C^*(k_z)C(k_z)\right)\,\mathrm{d}k_z,
\end{aligned} \tag{8}$$

where $P_d(\theta_n)$ denote elements on the main diagonal of $\mathcal{P}_\theta$. We have arrived at (8) using the unitaryness of the lifting transformation, the fact that $\mathcal{P}_\theta$ denotes a frequency representation of a spatially periodic operator, and a simple observation that as n and θ vary over $\mathbb{Z}$ and $[0,\,\Omega)$, respectively, $k_z = \theta_n = \theta + n\Omega$ assumes all values in $\mathbb{R}$. This expression for the $\mathcal{H}_2$ norm is particularly convenient

for comparison between the energy amplification of the uncontrolled and controlled systems.

III. Perturbation analysis of the $\mathcal{H}_2$ norm

Since we are dealing with bi-infinite matrices whose entries are operator valued, solving the Lyapunov equation in its original form is a difficult task. A discretization of the underlying operators in the wall-normal direction and truncation of bi-infinite matrices would yield a large-scale Lyapunov equation; determination of the solution to this equation for different values of θ and Ω is computationally expensive. Instead, we employ a much more efficient approach for solving (7) by utilizing a perturbation analysis [10], [11]. This method is well suited for systems in which spatially periodic terms are of small amplitude, and it results in a set of equations with a convenient structure. Namely, the $\mathcal{H}_2$ norm can be computed by solving a conveniently coupled system of operator valued Lyapunov and Sylvester equations. A finite dimensional approximation of the entries to these equations yields a set of algebraic matrix equations whose order is determined by the size of discretization in y.

The results of this section are derived for system (6) with block-diagonal operators $\mathcal{B}_\theta$ and $\mathcal{C}_\theta$, $\mathcal{A}_\theta := \mathcal{A}_{0\theta} + \alpha\mathcal{A}_{1\theta}$, where $\mathcal{A}_{0\theta}$ is a block-diagonal operator, $\mathcal{A}_{1\theta}$ is an operator with non-zero elements on the first block sub-diagonals, and $0 < \alpha \ll 1$. The structure of these operators for the linearized NS system is described in § II-B.

Following [10], [11], we define

$$\mathcal{P}_\theta \;:=\; \sum_{k=0}^{\infty} \alpha^k \mathcal{P}_{k\theta} \;=\; \mathcal{P}_{0\theta} \,+\, \alpha\mathcal{P}_{1\theta} \,+\, \alpha^2\mathcal{P}_{2\theta} \,+\, \cdots,$$

and compare equal powers of α in (7) to derive the a set of Lyapunov equations for self-adjoint operators $\{\mathcal{P}_{k\theta}\}_{k\,\in\,\mathbb{N}_0}$

$$\mathcal{A}_{0\theta}\mathcal{P}_{0\theta} \,+\, \mathcal{P}_{0\theta}\mathcal{A}_{0\theta}^* \;=\; -\,\mathcal{B}_\theta\mathcal{B}_\theta^*, \tag{9a}$$

$$\mathcal{A}_{0\theta}\mathcal{P}_{i\theta} \,+\, \mathcal{P}_{i\theta}\mathcal{A}_{0\theta}^* \;=\; -\,(\mathcal{A}_{1\theta}\mathcal{P}_{i-1,\theta} \,+\, \mathcal{P}_{i-1,\theta}\mathcal{A}_{1\theta}^*), \tag{9b}$$

with $i \geq 1$. Now, since both $\mathcal{B}_\theta\mathcal{B}_\theta^*$ and $\mathcal{A}_{0\theta}$ in (9a) are block-diagonal, so is $\mathcal{P}_{0\theta}$, $\mathcal{P}_{0\theta} := \operatorname{diag}\{P_{0,0}(\theta_n)\}_{n\,\in\,\mathbb{Z}}$, and $P_{0,0}(\theta_n)$ is determined from

$$A_0(\theta_n)P_{0,0}(\theta_n) \,+\, P_{0,0}(\theta_n)A_0^*(\theta_n) \;=\; -\,B(\theta_n)B^*(\theta_n).$$

Indices l and m in $P_{l,m}$ indicate that operator $P_{l,m}$ belongs to the mth upper block sub-diagonal of $\mathcal{P}_{l\theta}$; $m = 0$ denotes elements on the main diagonal. Since $\mathcal{P}_{0\theta}$ is block-diagonal and $\mathcal{A}_{1\theta}\mathcal{P}_{0\theta}$ has non-zero blocks only on the first sub-diagonals, by evaluating (9b) at $i = 1$, we observe that $\mathcal{P}_{1\theta}$ has the same structure as $\mathcal{A}_{1\theta}$, i.e.

$$\mathcal{P}_{1\theta} \;:=\; \mathcal{S}_1 \operatorname{diag}\{P_{1,1}(\theta_n)\}_{n\,\in\,\mathbb{Z}} \,+\, \operatorname{diag}\{P_{1,1}^*(\theta_n)\}_{n\,\in\,\mathbb{Z}}\,\mathcal{S}_1^*.$$

Thus, $\operatorname{trace}(\mathcal{P}_{1\theta}) \equiv 0$, and $P_{1,1}(\theta_n)$ satisfies

$$\begin{aligned} &A_0(\theta_{n-1})P_{1,1}(\theta_n) \,+\, P_{1,1}(\theta_n)A_0^*(\theta_n) \;=\\ &-\,(A_{-1}(\theta_n)P_{0,0}(\theta_n) \,+\, P_{0,0}(\theta_{n-1})A_1^*(\theta_n))\,. \end{aligned}$$

Observing the right hand side of (9b) for $i = 2$, we see that $\mathcal{A}_{1\theta}\mathcal{P}_{1\theta}$ has non-zero blocks only on the main diagonal and the second sub-diagonals. Since $\mathcal{A}_{0\theta}$ is block-diagonal, $\mathcal{P}_{2\theta}$ has the same structure as $\mathcal{A}_{1\theta}\mathcal{P}_{1\theta}$, i.e.

$$\begin{aligned} \mathcal{P}_{2\theta} \;&:=\; \operatorname{diag}\{P_{2,0}(\theta_n)\}_{n\,\in\,\mathbb{Z}} \,+\, \mathcal{S}_2 \operatorname{diag}\{P_{2,2}(\theta_n)\}_{n\,\in\,\mathbb{Z}} \,+\\ &\qquad \operatorname{diag}\{P_{2,2}^*(\theta_n)\}_{n\,\in\,\mathbb{Z}}\,\mathcal{S}_2^*,\\ \mathcal{S}_2 \;&:=\; \mathcal{S}_1^2 \;=\; \operatorname{toep}\{\cdots, 0, 0, 0, \boxed{0}, 0, I, 0, \cdots\}. \end{aligned}$$

The self-adjoint operator $P_{2,0}(\theta_n)$ satisfies the following Lyapunov equation

$$\begin{aligned} &A_0(\theta_n)P_{2,0}(\theta_n) \,+\, P_{2,0}(\theta_n)A_0^*(\theta_n) \;=\\ &-\,(A_1(\theta_n)P_{1,1}(\theta_n) \,+\, P_{1,1}^*(\theta_n)A_1^*(\theta_n) \,+\\ &A_{-1}(\theta_{n+1})P_{1,1}^*(\theta_{n+1}) \,+\, P_{1,1}(\theta_{n+1})A_{-1}^*(\theta_{n+1})), \end{aligned}$$

and $P_{2,2}(\theta_n)$ satisfies the following Sylvester equation

$$\begin{aligned} &A_0(\theta_{n-2})P_{2,2}(\theta_n) \,+\, P_{2,2}(\theta_n)A_0^*(\theta_n) \;=\\ &-\,(A_{-1}(\theta_{n-1})P_{1,1}(\theta_n) \,+\, P_{1,1}(\theta_{n-1})A_1^*(\theta_n)). \end{aligned}$$

Furthermore, for any $k \in \mathbb{N}$, the structure of operators $\mathcal{A}_{0\theta}$, $\mathcal{A}_{1\theta}$, and $\mathcal{P}_{i-1,\theta}$ in (9b) implies

$$\begin{aligned} \mathcal{P}_{2k-1,\theta} \;&=\; \sum_{m=1}^{k} \mathcal{S}_{2m-1} \operatorname{diag}\{P_{2k-1,2m-1}(\theta_n)\}_{n\,\in\,\mathbb{Z}} \,+\\ &\qquad \sum_{m=1}^{k} \operatorname{diag}\{P_{2k-1,2m-1}^*(\theta_n)\}_{n\,\in\,\mathbb{Z}}\,\mathcal{S}_{2m-1}^*,\\ \mathcal{P}_{2k,\theta} \;&=\; \operatorname{diag}\{P_{2k,0}(\theta_n)\}_{n\,\in\,\mathbb{Z}} \,+\\ &\qquad \sum_{m=1}^{k} \mathcal{S}_{2m} \operatorname{diag}\{P_{2k,2m}(\theta_n)\}_{n\,\in\,\mathbb{Z}} \,+\\ &\qquad \sum_{m=1}^{k} \operatorname{diag}\{P_{2k,2m}^*(\theta_n)\}_{n\,\in\,\mathbb{Z}}\,\mathcal{S}_{2m}^*, \end{aligned}$$

with $\mathcal{S}_m := \mathcal{S}_1^m$. The equations for operators $P_{l,m}(\theta_n)$ are easily obtained by elementwise comparison of bi-infinite matrices on both sides of (9b). These equations and the above derivations are summarized in Proposition 1.

Proposition 1: The $\mathcal{H}_2$ norm of system (6) with $\mathcal{A}_\theta := \mathcal{A}_{0\theta} + \alpha\mathcal{A}_{1\theta}$, block diagonal operators $\{\mathcal{B}_\theta, \mathcal{C}_\theta, \mathcal{A}_{0\theta}\}$, $0 < \alpha \ll 1$, and

$$\mathcal{A}_{1\theta} \;=\; \mathcal{S}_1 \operatorname{diag}\{A_{-1}(\theta_n)\}_{n\,\in\,\mathbb{Z}} \,+\, \operatorname{diag}\{A_1(\theta_n)\}_{n\,\in\,\mathbb{Z}}\,\mathcal{S}_1^*,$$

is determined by

$$\begin{aligned} ||\mathcal{H}||_2^2 \;&=\; \frac{1}{2\pi}\int_{-\,\infty}^{\infty} \left[\|\mathcal{H}\|_2^2\right](k_z)\,\mathrm{d}k_z,\\ \left[\|\mathcal{H}\|_2^2\right](k_z) \;&=\; \sum_{k=0}^{\infty} \alpha^{2k} \operatorname{trace}(P_{2k,0}(k_z)C^*(k_z)C(k_z)), \end{aligned}$$

where

$$\begin{aligned} &A_0(\theta_n)P_{0,0}(\theta_n) \,+\, P_{0,0}(\theta_n)A_0^*(\theta_n) \;=\; -\,B(\theta_n)B^*(\theta_n),\\ &A_0(\theta_n)P_{2k,0}(\theta_n) \,+\, P_{2k,0}(\theta_n)A_0^*(\theta_n) \;=\\ &-\,(A_1(\theta_n)P_{2k-1,0}(\theta_n) \,+\, P_{2k-1,1}^*(\theta_n)A_1^*(\theta_n) \,+\\ &A_{-1}(\theta_{n+1})P_{2k-1,1}^*(\theta_{n+1}) \,+\, P_{2k-1,1}(\theta_{n+1})A_{-1}^*(\theta_{n+1})),\\ &A_0(\theta_{n-l})P_{l,l}(\theta_n) \,+\, P_{l,l}(\theta_n)A_0^*(\theta_n) \;=\\ &-\,(A_{-1}(\theta_{n-l+1})P_{l-1,l-1}(\theta_n) \,+\, P_{l-1,l-1}(\theta_{n-1})A_1^*(\theta_n)),\\ &A_0(\theta_{n-m})P_{l,m}(\theta_n) \,+\, P_{l,m}(\theta_n)A_0^*(\theta_n) \;=\\ &-\,(A_1(\theta_{n-m})P_{l-1,m+1}(\theta_n) \,+\, P_{l-1,m+1}(\theta_{n+1})A_{-1}^*(\theta_{n+1}) \,+\\ &A_{-1}(\theta_{n-m+1})P_{l-1,m-1}(\theta_n) \,+\, P_{l-1,m-1}(\theta_{n-1})A_1^*(\theta_n)), \end{aligned}$$

$$m \;=\; \begin{cases} 2,4,\ldots,l-2 & l \;-\; \text{even}, \\ 1,3,\ldots,l-2 & l \;-\; \text{odd}. \end{cases}$$

Remark 1: Notation θ_{n-l} in Proposition 1 represents a shortcut for $k_z - l\Omega$, i.e. $\theta_{n-l} := \theta + (n-l)\Omega = \theta_n - l\Omega = k_z - l\Omega$.

IV. Energy amplification of the 2D/3C model

We next study the energy amplification of stochastically excited 2D/3C model (6). In this special case, the Lyapunov and Sylvester equations in Proposition 1 can be rewritten in an R-independent form which results in an explicit expression for the $\mathcal{H}_2$ norm in terms of the Reynolds number R. We discuss the energy amplification dependence on k_z and Ω and demonstrate that the arrays of counter-rotating streamwise vortices of appropriately selected amplitude and frequency have a potential for reducing the energy amplification of the uncontrolled flow.

Our main result, establishes a formula for the energy amplification of streamwise constant perturbations in parallel channel flows $U(y)$ subject to an array of counter-rotating streamwise vortices (3) with a small amplitude α, $\alpha := R_w/R \ll 1$. The proof of Theorem 2 is omitted due to page constraints and will be reported elsewhere.

Theorem 2: For any parallel channel flow $U(y)$ subject to an array of counter-rotating streamwise vortices (3) with $\alpha := R_w/R \ll 1$, the energy amplification of streamwise constant perturbations is given by

$$\begin{aligned} \|\mathcal{H}\|_2^2 \;&=\; \frac{1}{2\pi}\int_{-\infty}^{\infty} \left[\|\mathcal{H}\|_2^2\right](k_z)\,\mathrm{d}k_z, \\ \left[\|\mathcal{H}\|_2^2\right](k_z) \;&=\; \Big(f_0(k_z) + \sum_{k=1}^{\infty} R_w^{2k} f_{2k}(k_z,\Omega)\Big)\,R + \\ &\qquad \Big(g_0(k_z) + \sum_{k=1}^{\infty} R_w^{2k} g_{2k}(k_z,\Omega)\Big)R^3. \end{aligned}$$

Theorem 2 represents the basis for our next discussion on the effectiveness of the controls given by (3). f and g in Theorem 2 are determined by the traces of the solutions to certain operator Lyapunov equations. The f-functions are the same for *all* parallel channel flows $U(y)$, and the g-functions depend on the underlying parallel flow through their dependence on the nominal shear $U_y(y)$. For the large-Reynolds-number flows the energy amplification is mostly influenced by $g_0(k_z)$ and $g_{2n}(k_z,\Omega)$; this is an immediate consequence of the $O(R^3)$ scaling in Theorem 2.

Fig. 2 shows how f_0 and g_0 change with k_z. These functions are independent of Ω and they determine the $\mathcal{H}_2$ norm of the uncontrolled flow. The exact value of the energy amplification in the uncontrolled system is given by a scaled summation of these two functions with the coefficients determined by R and R^3. This result was originally established by Bamieh & Dahleh [6] and it implies that the energy amplification of the large-Reynolds-number flows roughly follows the trend of g_0. We note that g_0 peaks at $k_z \approx 1.78$ which determines the prevalent spanwise length scale.

Plots of $f_2(k_z,\Omega)$ and $g_2(k_z,\Omega)$ from Theorem 2 are also shown in Fig. 2. From the plot of g_2 we see that a spanwise periodic sensorless flow control strategy (3) has a potential for decreasing the amount of energy amplification. Up to a second order in R_w, the largest suppression of the energy amplification takes place in the regions of spanwise wavenumbers where frequency responses of the uncontrolled system achieve their maxima. Moreover, as indicated by the dark-blue regions in the plot of g_2, this suppression gets larger as Ω increases but it rapidly flattens and reaches a very slow rate of change for Ω larger than ≈ 30.

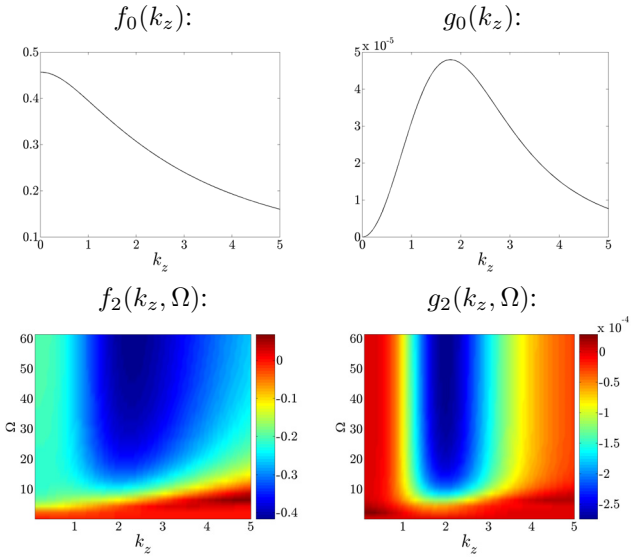

Fig. 2. Plots of functions f_0, g_0, f_2, and g_2 in Theorem 2. The g-functions are shown in plane channel flow.

The (k_z,Ω)–dependence of functions g_4, g_6, g_8, and g_{10} in plane channel flow is shown in Fig. 3. These plots indicate that the higher order corrections to the $\mathcal{H}_2$ norm generate alternating positive and negative contributions to the energy amplification, but otherwise follow the general trends observed in the plot of g_2. We also note a progressive increase in the magnitude of the higher order corrections, which necessitates a judicious choice of R_w in Theorem 2 to guarantee convergence.

The plots in Fig. 4 show the k_z-parameterized $\mathcal{H}_2$ norms of the uncontrolled plane channel flow with $R = 2000$ (blue curves) and the flow subject to (3) with $\{R_w = 0.25,\ \Omega = 61.48\}$ (left plot) and $\{R_w = 0.3,\ \Omega = 61.48\}$ (right plot). The energy amplification of the controlled flow is obtained using Theorem 2 by approximating the infinite summations in the expression for $\left[\|\mathcal{H}\|_2^2\right](k_z)$ by the summations with: one term (green curves), two terms (red curves), three terms (cyan curves), four terms (magenta curves), and five terms (black curves), respectively. Clearly, for selected values of R_w and Ω, the second order corrections to the $\mathcal{H}_2$ norm give optimistic estimates of the energy amplification reduction that can be achieved with an array of counter-rotating streamwise vortices. In the left plot, the curves corresponding to the sixth, eight, and tenth order corrections lie almost on the top of each other. These results closely match the results obtained using large-scale computations (not shown here), and indicate that the largest energy amplification of the uncontrolled flow is reduced by approximately 25 % with $\{R_w = 0.25,\ \Omega = 61.48\}$. This demonstrates the

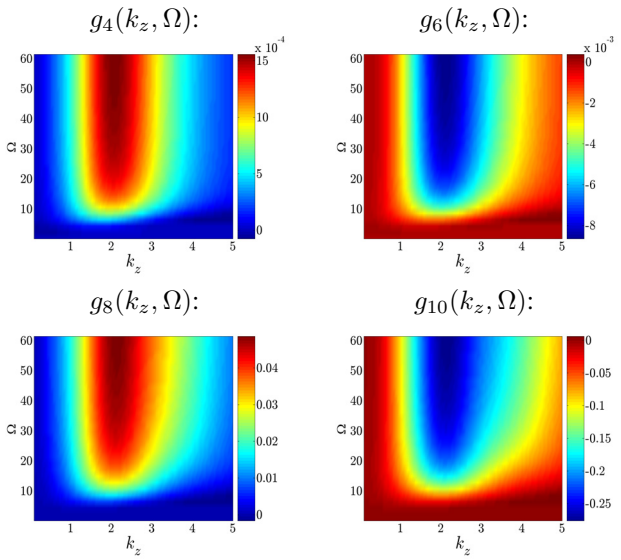

Fig. 3. Plots of functions g_4, g_6, g_8, and g_{10} in plane channel flow.

ability of control strategy (3) to significantly weaken the most energetic structures in transitional channel flows. Finally, we note that the truncations obtained using the fourth order corrections yield somewhat conservative estimates, but these estimates are much closer to the true values of the energy amplification than the estimates obtained using the second order corrections.

The right plot in Fig. 4 illustrates the slower rate of convergence of our method for larger values of R_w; by increasing the amplitude of oscillations even further, the perturbation analysis may fail to converge. In spite of this, the procedure presented here is capable of identifying important trends in amplification of stochastic disturbances and thereby providing systematic guidelines for a selection of control parameters in (3).

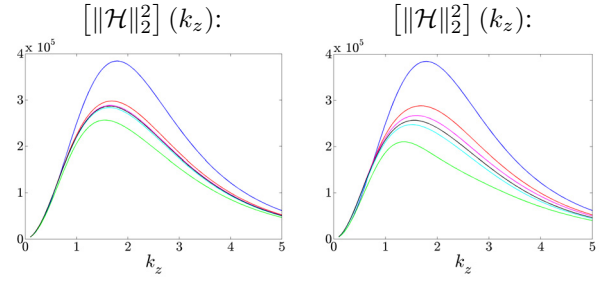

Fig. 4. The energy amplification in plane channel flow with $R = 2000$, $\{R_w = 0.25, \Omega = 61.48\}$ (left), and $\{R_w = 0.3, \Omega = 61.48\}$ (right). The blue curves denote the uncontrolled flow; the controlled flow plots are obtained using Theorem 2 with the infinite summations approximated by the summations with: 1 (green), 2 (red), 3 (cyan), 4 (magenta), and 5 (black) terms, respectively.

V. Concluding Remarks

This paper develops a system theoretic paradigm for modeling, optimization, and evaluation of *spatially periodic sensorless flow control strategies* in wall-bounded shear flows. The new paradigm represents a spatial analog of the well-known principle of *vibrational control* [14], where the system's dynamical properties are altered by introducing zero-mean vibrations into the system's coefficients. Depending on the relationship between the natural modes of the uncontrolled system and the forcing frequency, the vibrational control may have a potential for providing stability of the overall system and for changing its input-output norms. For example, it is well known that the inverted pendulum can be stabilized by sensorless means using high frequency oscillations of the suspension point [14]. We show that the principle of vibrational control can be also utilized in systems governing the dynamics of flow fluctuations in channel flows, where coefficients multiplying system's state have spatial periodicity. The key observation is that there is a potential for changing dynamical properties of the linearized NS equations (in favorable or unfavorable manner) whenever controls with spatial periodicity enter into the system's coefficients.

We model and analyze the influence of small amplitude streamwise vortices on energy amplification in channel flows. We develop models that govern the dynamics of flow fluctuations. Our results provide a theoretical explanation as to why *properly designed* arrays of counter-rotating streamwise vortices can reduce the energy amplification in channel flows.

In our future efforts we will: a) investigate the optimal ratio between the control amplitude and frequency for turbulence suppression; b) employ our analysis to highlight the physical mechanisms leading to turbulence suppression; c) test our results in direct numerical simulations of the NS equations.

References

[1] W. Schoppa and F. Hussain, "Large-scale control strategy for drag reduction in turbulent boundary layers," *Phys. Fluids*, vol. 10, no. 5, pp. 1049–1051, 1998.

[2] K. M. Butler and B. F. Farrell, "Three-dimensional optimal perturbations in viscous shear flow," *Phys. Fluids A*, vol. 4, p. 1637, 1992.

[3] L. N. Trefethen, A. E. Trefethen, S. C. Reddy, and T. A. Driscoll, "Hydrodynamic stability without eigenvalues," *Science*, vol. 261, pp. 578–584, 1993.

[4] B. F. Farrell and P. J. Ioannou, "Stochastic forcing of the linearized Navier-Stokes equations," *Phys. Fluids A*, vol. 5, no. 11, pp. 2600–2609, 1993.

[5] S. C. Reddy and D. S. Henningson, "Energy growth in viscous channel flows," *J. Fluid Mech.*, vol. 252, pp. 209–238, 1993.

[6] B. Bamieh and M. Dahleh, "Energy amplification in channel flows with stochastic excitation," *Phys. Fluids*, vol. 13, no. 11, pp. 3258–3269, 2001.

[7] P. J. Schmid and D. S. Henningson, *Stability and Transition in Shear Flows*. New York: Springer-Verlag, 2001.

[8] M. R. Jovanović, "Modeling, analysis, and control of spatially distributed systems," Ph.D. dissertation, University of California, Santa Barbara, 2004.

[9] M. R. Jovanović and B. Bamieh, "Componentwise energy amplification in channel flows," *J. Fluid Mech.*, vol. 534, pp. 145–183, July 2005.

[10] M. Fardad and B. Bamieh, "A perturbation approach to the H_2 analysis of spatially periodic systems," in *Proceedings of the 2005 American Control Conference*, Portland, OR, 2005, pp. 4838–4843.

[11] ——, "Perturbation methods in stability and norm analysis of spatially periodic systems," *SIAM Journal on Control and Optimization*, 2006, submitted.

[12] R. C. DiPrima and G. J. Habetler, "A completeness theorem for non-selfadjoint eigenvalue problems in hydrodynamic stability," *Arch. Rat. Mech. Anal.*, vol. 34, pp. 218–227, 1969.

[13] M. Fardad, M. R. Jovanović, and B. Bamieh, "Frequency analysis and norms of distributed spatially periodic systems," *IEEE Transactions on Automatic Control*, 2005, submitted.

[14] S. M. Meerkov, "Principle of vibrational control: theory and applications," *IEEE Trans. Autom. Control*, vol. AC-25, no. 4, pp. 755–762, 1980.